Prediction of the fuel economy potential for a skutterudite thermoelectric generator in light-duty vehicle applications

Song Lan, Zhijia Yang, Richard Stobart, Rui Chen*

Department of Aeronautical and Automotive Engineering, Loughborough University, UK

HIGHLIGHTS

- Developed and validated a semi-empirical model for fuel saving estimation.
- Fuel saving of a thermoelectric generator used in light-duty vehicle was investigated.
- Thermoelectric generator integration effects has been identified and analysed.
- Installation position has a significant influence on the fuel saving potential.
- DC-DC convector and added weight are the main effects to fuel saving reduction.

ARTICLE INFO

ABSTRACT

Thermoelectric generators (TEGs) have the characteristics of low maintenance, silent operation, stability, and compactness, which make them outstanding devices for waste heat recovery in light-duty vehicles. Significant strides have been made in the high temperature (300–800 °C) thermoelectric materials and recent work is beginning to translate those material improvements into TEG performance. Recently developed modules that incorporate new, competitive formulations of skutterudite form the basis for this study. Vehicular TEGs have not had real commercial applications yet and faced commercialization challenges. Simply estimating the fuel saving potential from the TEG output is not sufficient and due consideration must also be given to the system integration effects. Thus, a new approach for predicting the fuel saving potential of a vehicular TEG while also considering integration effects is developed in this paper. The prediction is based on a recently developed high temperature skutterudite thermoelectric modules [1]. Based on this method, the benefit of a skutterudite TEG is investigated by balancing the benefits with the added complexity of a TEG and improvement measures are explored.

Based on two scenarios of the TEG integrated in different positions of a conventional light-duty vehicle, a semi-empirical model is developed, which includes a quasi-static vehicle model, a dynamic exhaust model, a dynamic coolant model, and a dynamic TEG model. Four integration effects: the additional mass, the power consumption of an electric circulation pump, the effect of exhaust back-pressure and the energy loss in the DC-DC converter, are studied in the semi-empirical model. The evaluation results show the TEG installation position has a significant influence on the fuel saving potential due to the higher quality of the exhaust gas. Placing the TEG closer to the exhaust manifold can increase fuel saving potential by 50%. The four integration effects taken together cause a 25% reduction of fuel saving potential. The energy loss in DC-DC convector and added weight are the main contributors to this reduction. An optimised design for the TEG installation operating under an optimised control strategy delivers a fuel consumption reduction of 4% over the constant-speed 120 km/h driving cycle.

1. Introduction

Based on the typical energy flow path of an internal combustion engine (ICE), approximately one third of the energy is discharged through the exhaust flow [2–4]. A thermoelectric generator (TEG) can convert a proportion of the otherwise wasted thermal energy of the exhaust gas to electricity directly for use in the vehicle systems. Higher degree of electrification is being driven by conventional ICE vehicles for

---

enhanced driving experience, safety and efficiency, making electric recovery more useful [5]. Besides, compared with other waste heat recovery (WHR) technologies such as organic Rankine cycle and turbo-compounding, TEG has the advantages of low maintenance, silent operation, stability, and compactness. All of these advantages in addition to the increasingly demanding CO_2 emissions requirements for passenger cars [6] make the TEG an attractive option for conventional light-duty vehicles. Nevertheless, considerable technical challenges for TEG integration remain. The two main challenges include:

- Low conversion efficiency and low maximum operating temperature dictated by the properties of the chosen thermoelectric materials
- Integration effects arising from increased mass, increased exhaust backpressure, and installation complexity

Many efforts have been made in the development of improved thermoelectric materials during the last few years. Bismuth telluride (Bi_2Te_3) is the well-known thermoelectric material and has already been proposed for WHR. Car manufacturers and their suppliers have successfully demonstrated the use of Bi_2Te_3 in TEG systems [7]. However due to the limit that the use of Bi_2Te_3 places on the hot side temperature, an exhaust by-pass proved necessary. Since a lot of thermal energy at high temperature escaped without recovery, the efficiency of the Bi_2Te_3 TEGs were less than 5% [7–9]. Thus, the most promising and practical materials for a vehicular TEG in WHR would be materials designed to withstand high temperatures. This means larger temperature gradients can be achieved with this material and thus more power and higher efficiency could be potentially achieved. Skutterudite thermoelectric materials have shown good potential for higher efficiency at higher temperature (500 °C) based on a number of recent material and module test results. Garcia et al. [10] fabricated skutterudite module, which provides more than $1.5\,W\,cm^{-3}$ volume power density at a temperature difference of 365 K. Nie et al. [11] demonstrated excellent stability of their skutterudite module with 7.2% conversion efficiency. Yang et al. developed skutterudite module with $1.4\,W\,cm^{-3}$ volume power density at a temperature difference of 365 K [1]. The operating temperature range of skutterudite is better matched to automotive applications, especially for gasoline engines. Consequently, an increased TEG efficiency can be expected. Recent work is beginning to translate those material improvements into TEG performance. Compared with the strides in thermoelectric materials development, the integration challenges have also been studied. Since the TEG represents another component in the exhaust system, its integration presents challenges. The fuel economy benefit could be compromised through a number of integration effects:

- Added mass
- Power consumption of an electric circulation pump
- Increased exhaust backpressure
- Energy loss in DC-DC converter

All of the listed effects above may lead to a significant reduction in the fuel saving potential of a TEG in vehicle application. Rowe et al. [12] identified the added weight penalty for a TEG applied in a 1.5L family car. For a 13 kg mass TEG, at least 156 W electrical power had to be generated in order to compensate for its added weight penalty. Li et al. [13] proposed a novel design for a concentric cylindrical TEG system for use in the automotive exhaust system with a compact and lightweight heat sink. Instead of using a bulky and heavy heat exchanger, this innovative design combined the heat pipes with heat exchanger, which reduced the weight of the TEG system and the whole vehicle as well, consequently improving the fuel economy. Deng et al. [14] investigated the compatibility of engine-cooling system when a TEG cooling unit was integrated. Based on both simulation and experimental data, it was found out that the temperature of the integrated cooling system is 5 °C more than that of the primary engine cooling

system. More powerful water pump and cooling fans were recommended to reduce the effect of the TEG cooling unit. He et al. [15] optimized the heat exchanger of TEG by considering engine power loss caused by exhaust backpressure. It was found out that the engine power loss increased linearly with exhaust backpressure and the influence of backpressure could be reduced by optimizing the dimensions of the hot side heat exchanger. Cao and Peng [16] proposed a multiphase multi-level DC-DC conversion networks based on a 630 W TEG prototype for automotive applications. The proposed DC-DC conversion networks could effectively reduce the power loss in DC-DC converter from 5% of total TEG power output to about 3%.

This view of the literature strongly suggests that integration effects are sufficiently significant that they must be taken into account in evaluating the potential fuel economy improvement. However, the integration effects are usually neglected in the TEG performance prediction [17–19]. Therefore, the goal of the paper is to investigate, for the first time, the integration effects on the fuel saving potential of a skutterudite TEG applied in a light-duty conventional ICE vehicle. In contrast to the previous TEG performance prediction methods [17–19], which only predicts the electric power output, this proposed approach can further estimate the fuel saving percentage of TEG. Another novelty of this paper is that relatively complete experimental validations are conducted with experiments on both engine and recent developed skutterudite TEG prototype.

2. TEG integration into a light-duty vehicle
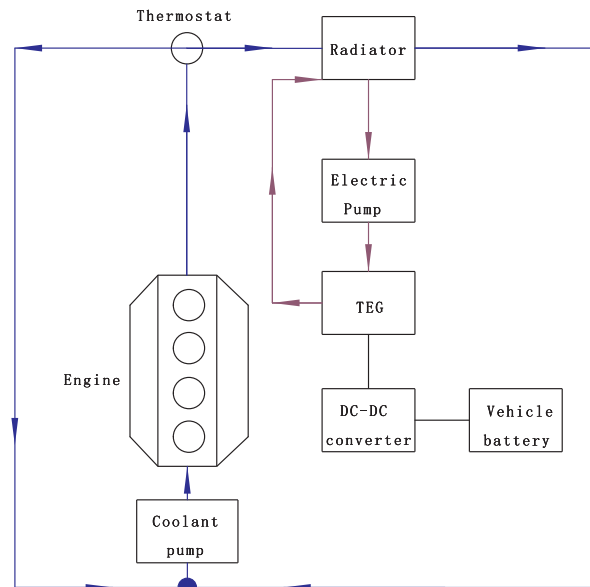
2.1. TEG integration scenario

New technology is usually firstly adopted in high-end cars and then gradually being used in standard cars. Consequently, for the purposes of this study, the TEG is assumed to be integrated in a 2 l-gasoline and D-segment passenger car whose specification is shown in Appendix A. The TEG integrated into the exhaust system converts part of the exhaust energy into electricity and through the DC-DC converter the regenerated electrical power is converted to fit the electric system of the car (Fig. 1(b)). Therefore, the load on the alternator is relieved and engine torque dragging the alternator is reduced, so is the fuel consumption. The method of calculation to quantify this fuel consumption reduction will be detailed later in this paper.

There are a few possible installation positions for the TEG in the exhaust line, such as upstream of the three-way catalytic (TWC), downstream of the TWC, and downstream of the muffler. Considering the optimal efficiency of the skutterudite materials in its temperature range, positioning the skutterudite TEG downstream the muffler significantly reduces the available exhaust gas temperature and conversion efficiency. Thus, with a typical gasoline engine exhaust system featuring a close-coupled catalyst (CCC) and a main TWC, there are two conceivable TEG installation positions: between CCC and main TWC (scenario 1) and downstream of main TWC (scenario 2). Fig. 1(a) shows the integration scenarios of TEG in the exhaust line.

Apart from the integration of TEG in the exhaust line, the TEG also needs to be integrated with the vehicular cooling circuit, which absorbs the heat drawn from the exhaust gas. The lower the coolant intake temperature of TEG, the higher the electric power output of the TEG. Thus, maintaining the cold side temperature of TEG with cold coolant from the radiator outlet is set as the integration scenario for both scenario 1 and scenario 2. The operation of thermostat valve can prevent coolant from flowing to the TEG. Thus, an electrical water pump is added to form an independent coolant circuit. As can be seen from Fig. 1(b) that the added electrical water pump circulates the coolant through the cold side of TEG and the radiator. The heat from the engine and the TEG are both rejected to the ambient air through the radiator.
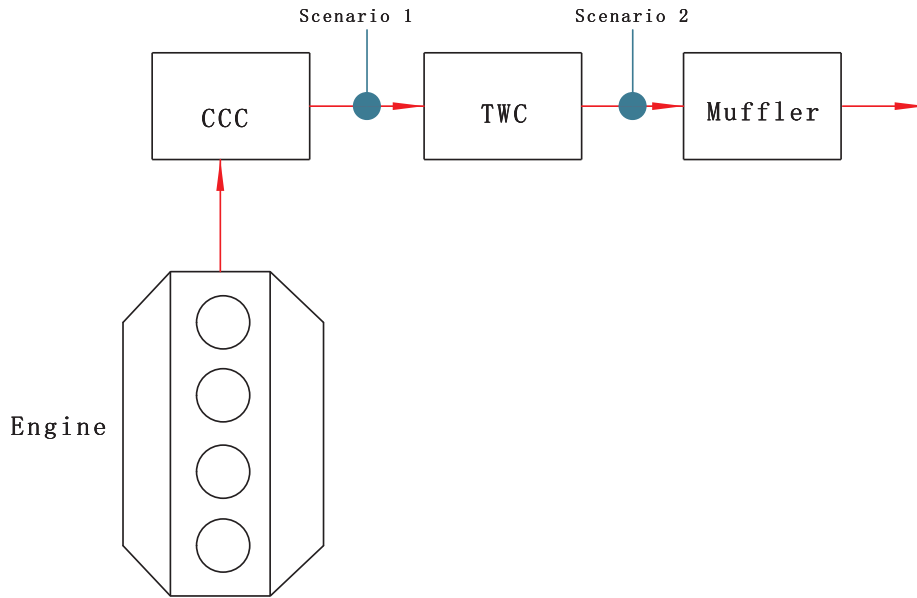
(a) Integration scenarios of TEG in the exhaust line.

(b) Integration scenarios of TEG in the cooling circuit.

Fig. 1. Integration scenarios of TEG in the light-duty passenger car.

2.2. TEG system structure

A typical TEG system comprises three components: a hot side heat exchanger, a cold side heat exchanger and thermoelectric modules (TEMs). The hot side and cold side heat exchanges (HXRs) are respectively connected to the exhaust path and coolant circuit. The TEMs are compressed in certain pressure between the hot side and cold side HXRs to ensures a stable thermal contact and reduce thermal contact resistance. The TEG can be design in different shapes (shaped as a rectangle, hexagon, cylindrical, etc.) and different size with a number of heat exchanger channels and TEMs [20]. Identifying the ideal size and shape of TEG needs a system-level optimization maximizing the power output while also considering the system costs [21]. In this paper, fuel saving prediction is the main target and the structural optimization is not considered. By simply restricting the TEG to 'shoe-box size', an unoptimized TEG with two channels of parallel counter-flow HXRs is proposed in this paper.

Fig. 2 shows the structure of the TEG system and its parameters are shown in Appendix A. As can be seen from Fig. 2, the TEG is mainly made up of counter-flow heat HXRs and in total 400 skutterudite TEMs. The TEG can be divided into two channels with four layers of TEMs, two hot side HXRs and three cold side HXRs. The size of TEG is constrained to 24 cm × 17 cm × 9.5 cm with 10 × 10 TEMs on each layer. It is assumed all the TEMs in a layer are connected serially to form a section and all the four sections are connected in parallel. The skutterudite materials used here is recently developed by University of Reading. The maximum ZT of this material is 1.13 at 405 °C for the n-type material and 0.93 at 550 °C for the p-type material. These skutterudite materials are then fabricated into thermoelectric modules with dimensions 1.6 cm × 1.3 cm × 0.4 cm by Cardiff University. The parameters of the skutterudite modules are shown in Appendix A. More details of skutterudite materials and modules can be seen in Ref. [1].
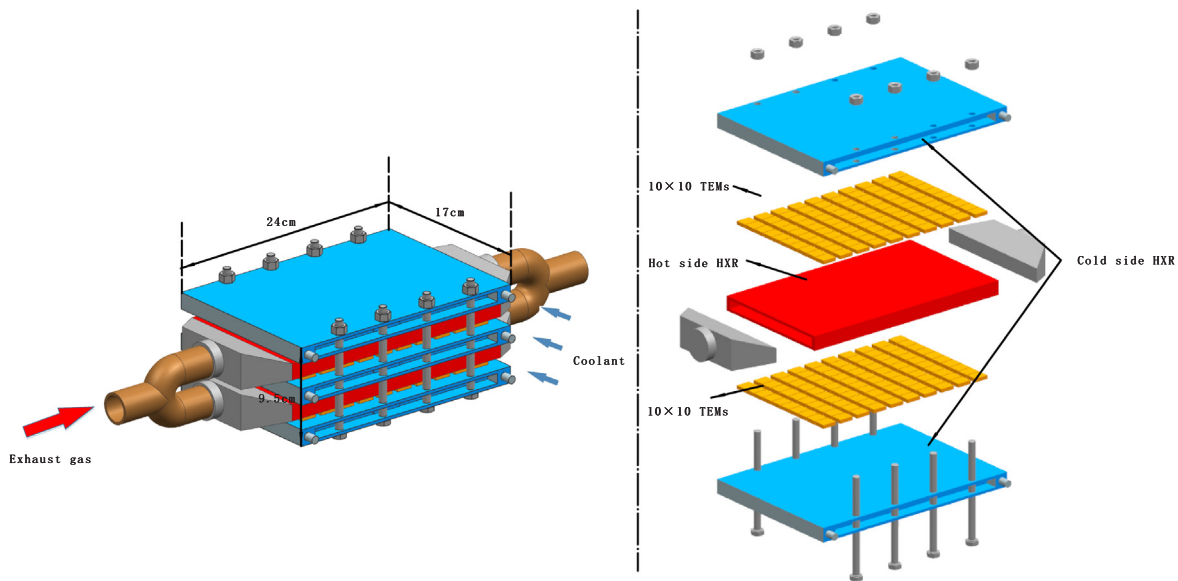
Fig. 2. The structure of TEG.

3. Method for TEG performance prediction

3.1. Experimental setup

In order to tune and validate the model, both a TEM test rig and a TEG engine test bench have been set up. The TEM test rig presented in Fig. 3 is the same as in Ref. [22], which is used to test skutterudite modules and validate the TEM model. Based on the integration scenario 2, a TEG engine test bench has also been established to tune and validate both the exhaust model and TEG model. The scheme of TEG engine test bench is shown in Fig. 4. The TEG is installed downstream of the TWC of the gasoline engine, which is the same as in the reference car. The exhaust pipe has been specially modified for the purposes of TEG research and a bypath is added so as to protect TEG from the effects of high temperature. This engine is installed on a test bench with a dynamometer which can be used to simulate different driving cycles. Instead of being integrated with the engine cooling system, the cold side temperature of the prototype TEG is maintained using chilled water from a laboratory recirculation chiller. Due to the limitations on the amount of thermoelectric material available for testing, only 12 skutterudite TEMs are placed on a hot side HXR, which has the same dimension as in the integration scenarios. In order to balance the energy distribution, a same size ceramic plate is placed on the other side of hot side HXR. While only one channel (a hot side HXR and two cold side

Fig. 3. TEM test rig.

HXRs) has been tested. Here it is assumed that the TEG engine test of one channel is representative and the power output can be scalable according to the number of channels.

The temperatures of exhaust gas ($T_{exh.in}$ and $T_{exh.out}$), coolant ($T_{col.in}$ and $T_{col.out}$), hot and cold side of the TEG (T_{hd} and T_{cd}) are measured by a number of thermocouple sensors with maximum uncertainty of 1 K. The flow rates of exhaust gas ($\dot{m}_{TEG.exh}$) and coolant ($\dot{m}_{TEG.col}$) are measured by flow meters with maximum uncertainty 0.1%. The data acquisition system used in the experimental work consists of an NI CRIO chassis and a 16 bit analog input module. It simultaneously records the data of all the temperatures, flow rates and output voltage ($U_{TEG.out}$) and current (I). The uncertainty for voltage and current measurements are respectively ± 0.05 A and ± 0.05 V.

3.2. Semi-empirical model development

Since a vehicle equipped with a TEG was not available, a semi-empirical model is developed according to the integration scenarios. Both experimental and published data are used to tune and validate the model. The semi-empirical model of TEG in passenger vehicle is made up by four sub-models: a quasi-static vehicle model [23], a dynamic exhaust model [24], a dynamic coolant model [25] and a dynamic TEG model [22]. The model structure and variables are shown Fig. 5. The quasi-static vehicle model is used to calculate the engine's load and speed and fuel consumption based on the chosen driving cycle. The exhaust model, coolant model and the TEG model are modelled dynamically. The exhaust mass flow rate ($\dot{m}_{TEG.exh}$) and temperature ($T_{exh.in}$) and coolant mass flow rate ($\dot{m}_{TEG.col}$) and temperature ($T_{col.in}$) are computed at the dynamic exhaust and coolant model based on the mass flow rate of fuel consumption ($\dot{m}_{fuel}$), engine speed (ω_{ic}) and torque (Tq_{ic}). The TEG model predicts the energy transfer from exhaust gas into electrical power ($P_{TEG.out}$). The development and validation of the three sub-modes are described in following subsections.

3.2.1. Quasi-static vehicle model

The modelling of the reference passenger car is carried out using the Quasi Static Simulation (QSS) toolkit [23], which is based on a library of Simulink blocks. The model structure is presented in Fig. 5 and the parameters for the reference cars are listed in Appendix A.

Based on a given driving cycle profile, the vehicle speed (v) can be readily converted into wheel revolution speed (ω_w) and traction torque (Tq_w) and then propagated back to the transmission block.

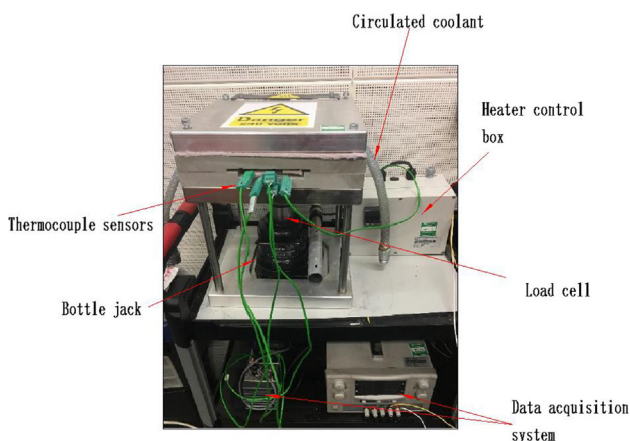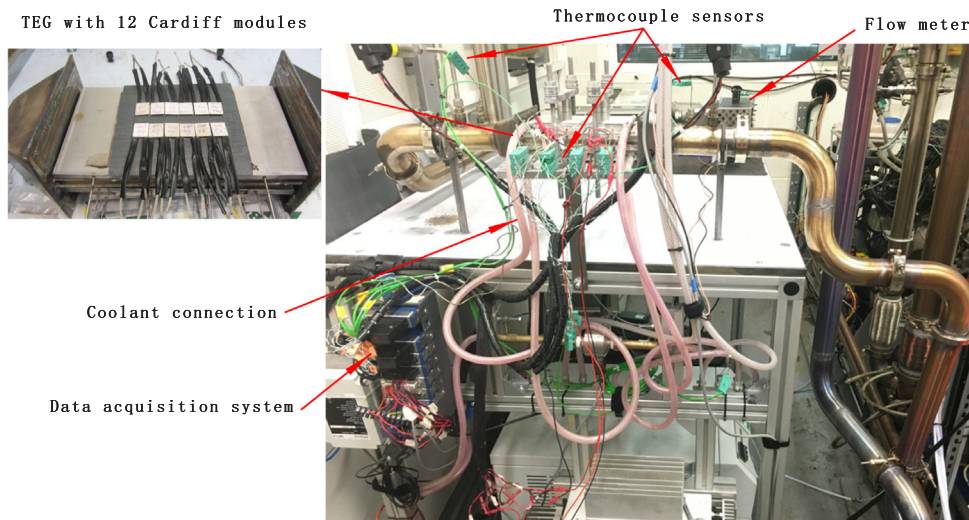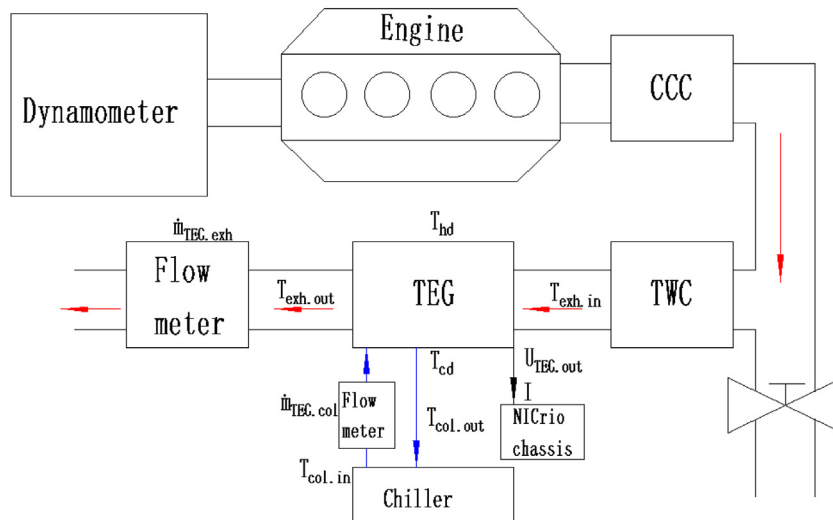(a) TEG engine test bench.

(b) TEG engine test bench structured diagram.

Fig. 4. The TEG engine test bench and its structure diagram.

$$Tq_w = r_{wh}F_v + \Theta_v a/r_{wh} \qquad (1)$$

$$\omega_w = v/r_{wh} \qquad (2)$$

where r_{wh}, F_v, Θ_v, a are respectively wheel diameter, force to drive the vehicle, vehicle total inertia, and vehicle acceleration.

By assuming values for the final drive ratio and efficiency, the

rotational speed (ω_{ic}) and torque (Tq_{ic}) of the engine are calculated. Once both ω_{ic} and Tq_{ic} have been determined, an engine fuel consumption map can be used to find the instantaneous fuel consumption rate ($\dot{m}_{fuel}$). Finally, $\dot{m}_{fuel}$ is integrated over the driving cycle to obtain the cumulative fuel consumption of the driving cycle (E_{fuel}).
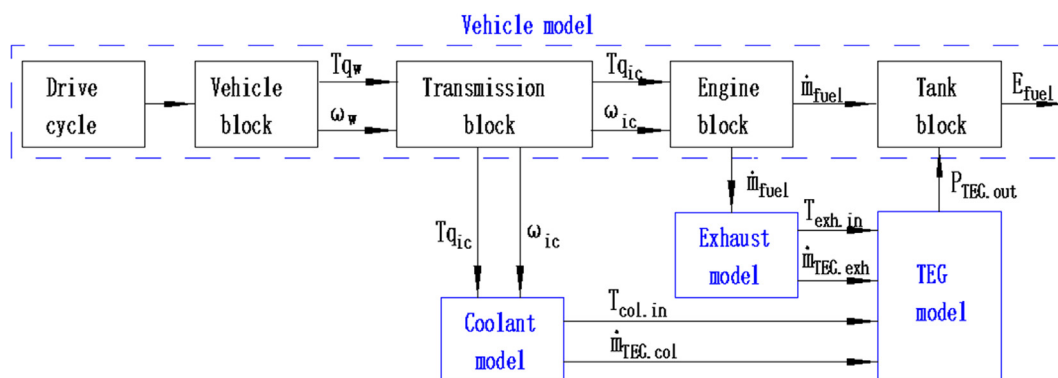

Fig. 5. Model structure and variables.

$$\dot{m}_{fuel} = f_{ic}(Tq_{ic}, \omega_{ic}) \tag{3}$$

$$E_{fuel} = \int_0^t \dot{m}_{fuel} dt \tag{4}$$

More details of this quasi-static vehicle model can be seen in Refs. [26,27]. This quasi-static approach has been demonstrated to give a reasonable accuracy for the fuel consumption [28]. The validation of the quasi-static vehicle model was conducted and it was found that the prediction for fuel consumption from the model was within the 2% of the published data for the NEDC [29]. Because the backward simulation method does not employ iteration, the quasi-static vehicle model runs relatively quickly. However, since the engine map is usually based on steady-state real world testing results, the vehicle model does not include engine and driveline dynamic effects. Because of their relatively small effect on the fuel economy estimation, such effects can be neglected for the overall assessment of fuel economy.

3.2.2. Dynamic exhaust model

The exhaust model is used to predict the inlet exhaust temperature $T_{exh.in}$ and exhaust flow rate $m_{TEG.exh}$ of the TEG system. Since no bypass rote is adopted, the exhaust flow rate of TEG $m_{TEG.exh}$ equals to the exhaust flow rate of the exhaust system $\dot{m}_{exh}$, which can be estimated based on $\dot{m}_{fuel}$ from the vehicle model:

$$\dot{m}_{TEG.exh} = \dot{m}_{exh} = (1 + \lambda)\dot{m}_{fuel} \tag{5}$$

where λ is the air-fuel ratio.

T_{cly} is the temperature of fluid delivered by the cylinder to the exhaust manifold. From experimental data is has been seen that a linear model in many cases is a sufficient approximation for the temperature variations of the gases that goes from the cylinder into the exhaust manifold [24]. The expression for the T_{cly} can be expressed as [24]:

$$T_{cly} = k_{exh.0} + \dot{m}_{exh}k_{exh.1} \tag{6}$$

where $k_{exh.0}$ and $k_{exh.1}$ are tuning constants.

The sketch of the heat transfer in the exhaust pipe is shown in Fig. 6. It can be seen that the heat transfer from the exhaust gas (T_{cly}) to the pipe wall and ambient decreases the outlet temperature of exhaust gas ($T_{exh.in}$). By assuming that the exhaust flow through a straight pipe with constant surrounding temperature, $T_{exh.in}$ can be determined by solving a simple differential equation for the temperature drop of a fluid in a straight pipe [24].

$$T_{exh.in} = T_{wal} + (T_{cly} - T_{wal})e^{-\frac{h_{pip.exh}A_{pip.exh}}{\dot{m}_{exh}c_{exh}}} \tag{7}$$

where c_{exh}, $h_{pip.exh}$, $A_{pip.exh}$ and T_{wal}, are respectively the specific heat of the exhaust gas, heat transfer coefficient, heat transfer area and wall temperature of exhaust pipe.

The thermal inertia of the exhaust pipe is taken into consideration in the calculation of T_{wal} by using an ordinary differential equation [24]:

$$\frac{dT_{wal}}{dt}m_{wal}c_{wal} = \dot{Q}_i(T_{wal}, T_{cly}) - \dot{Q}_e(T_{wal}, T_{eng}, T_{amb}) \tag{8}$$

where and c_{wal} are respectively the mass and specific heat of the pipe wall. T_{eng} and T_{amb} are respectively the engine temperature and ambient
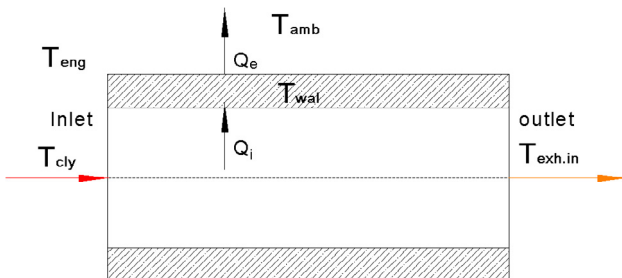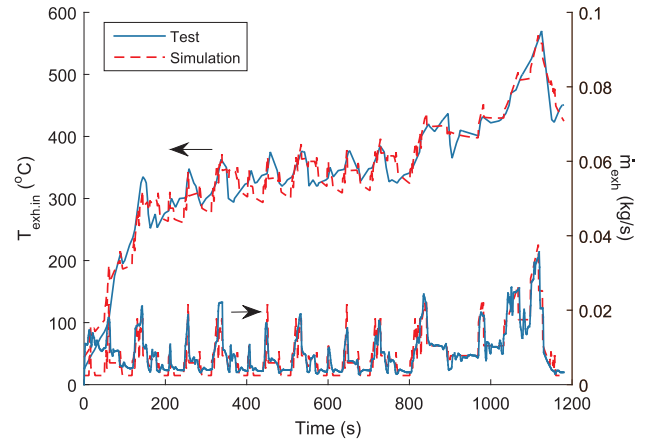

Fig. 7. Validation of dynamic exhaust model.

temperature. $\dot{Q}_i$ and $\dot{Q}_e$ are respectively the heat transferred from the exhaust to the wall and heat transferred from the wall to the ambient and engine and they can be expressed as follows [24]:

$$\dot{Q}_i = h_{g.i}A_{pip.exh}(T_{cly} - T_{wal}) \tag{9}$$

$$\dot{Q}_e = A_{pip.exh}[h_{cv.e}(T_{wal} - T_{amb}) + h_{cd.e}(T_{wal} - T_{eng}) + F_v \epsilon \sigma(T_{wal}^4 - T_{amb}^4)] \tag{10}$$

where $h_{g.i}$, $h_{cd.e}$ and $h_{cv.e}$ are respectively internal heat transfer coefficient, conductive heat transfer into the engine block, and convective heat transfer into the engine block. F_v is the gray body view factor, ϵ is the emissivity, and σ is the Stefan-Boltzmann constant.

Measurements for the exhaust data downstream of the TWC from the reference engine running the NEDC based on the referenced vehicle are used to tune and validate the exhaust model. A comparison of the modelled and measured $\dot{m}_{exh}$, $T_{exh.in}$ are respectively shown in Fig. 7. It can be seen that both $\dot{m}_{exh}$ and $T_{exh.in}$ correspond well with the test results, with mean absolute error around 8.4% and 5.1% respectively. $\dot{m}_{exh}$ has a minor influence on the power output of the TEG [30]. Therefore, the exhaust model can be considered validated and is used to provide accurate inputs for the dynamic TEG model.

3.2.3. Dynamic coolant model

Unlike the exhaust path, the engine coolant circuit is a closed circuit. Thus, the heat dissipated from the TEG can influence the cooling system. Before modelling the engine coolant, it is assumed that the heat rejected from the TEG system to the coolant circuit can be fully compensated by the added electrical water pump. Thus, the inlet temperature of the radiator is decided by the original engine coolant circuit.

According to the integration scenarios, the added electrical pump circulates the coolant through the radiator and TEG. The coolant flow rate of TEG $\dot{m}_{TEG.col}$ is assumed to be determined by the power output of the added electrical water pump (P_{pump}).

$$\dot{m}_{TEG.col} = P_{pump}k_{pump} \tag{11}$$

where k_{pump} is the tuning constant.

The sketch of the heat transfer in the engine coolant circuit is shown in Fig. 8. T_{col} is the engine coolant temperature at the inlet of the radiator and it can be modelled based on the coolant temperature model presented in Ref. [25]:

$$\dot{Q}_{rej.col} - \dot{Q}_{amb.col} - \dot{Q}_{rad.col} = \frac{dT_{col}}{dt}M_{col}c_{col} \tag{12}$$

where M_{col} and c_{col} are respectively the effective coolant mass and specific heat capacity of coolant. $\dot{Q}_{rej.col}$, $\dot{Q}_{amb.col}$ and $\dot{Q}_{rad.col}$ are respectively heat rejection to the coolant from engine, heat loss to the ambient and heat dissipation at the radiator. The details for the expressions of
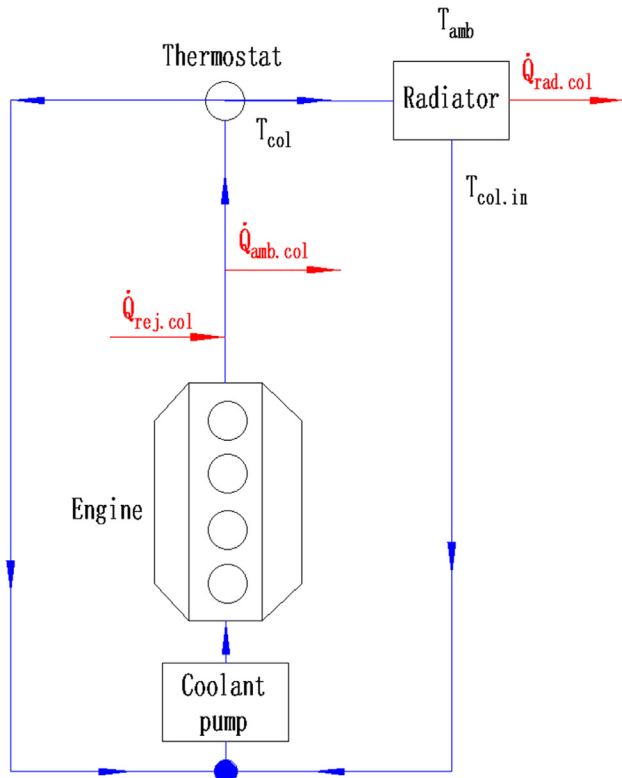

Fig. 6. Sketch of the heat transfer in the exhaust pipe.

Fig. 8. Sketch of the heat transfer in the engine coolant circuit.

$\dot{Q}_{rej.col}$, $\dot{Q}_{amb.col}$ and $\dot{Q}_{rad.col}$ can be seen in Ref. [25].

The outlet coolant temperature of radiator $T_{col.in}$, which is also the inlet coolant temperature of the TEG can then be expressed as:

$$T_{col.in} = T_{col} - \frac{A_{rad.col} h_{rad.col}}{\dot{m}_{rad.col} c_{col}} (T_{col} - T_{air}) \qquad (13)$$

where $h_{rad.col}$, $A_{rad.col}$, T_{air} and $\dot{m}_{rad.col}$ are respectively the radiator heat transfer coefficient, surface area of the radiator, ambient air temperature, coolant flow rate at radiator.

Since T_{col} are not available in the engine test bench. The NEDC test data for T_{col} from a Jaguar S-type vehicle [31], which is comparable to the reference vehicle, is used to tune and validate the coolant model. A comparison of the modelled and measured T_{col} is shown in Fig. 9. The average absolute error for T_{col} is 4.2%, which is sufficiently good to use as input for the TEG model.
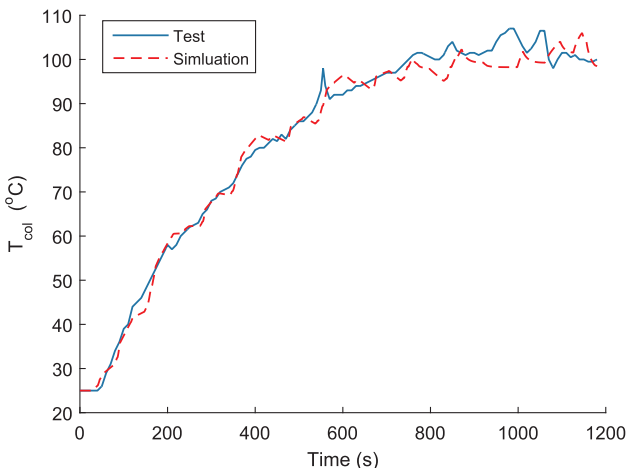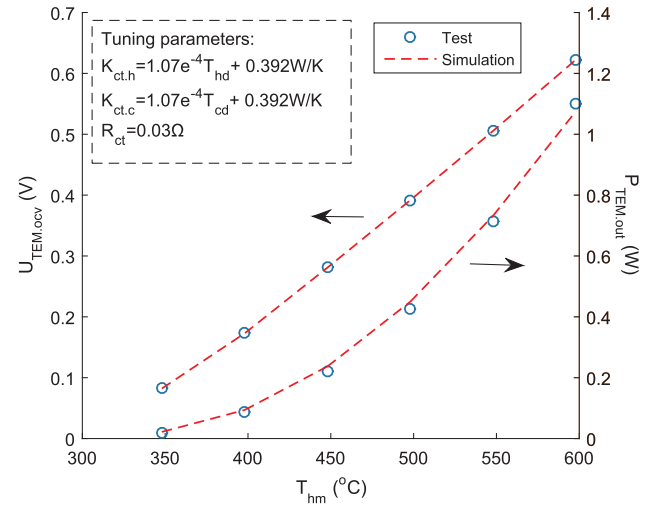

Fig. 9. Validation of dynamic coolant model.

Fig. 10. Validation of the TEM model.

3.2.4. Dynamic TEG model

The dynamic TEG model [22] developed previously by Loughborough University is used here as a sub-model for the semi-empirical vehicular TEG model. The TEG model can be divided into two models: a quasi-stationary TEM model and a dynamic TEG model. In this paper, all simulation settings not explicitly given are corresponding with the previous work. The model is built using respectively the properties of the skutterudite materials [1], the measured behaviour of the TEM and measurements made from the TEG engine test.

Measurements from the TEM test rig are used to tune and validate the skutterudite TEM model. The validation results and tuning parameters of thermal contact conductances ($K_{ct.h}$ and $K_{ct.c}$) and electrical contact resistances (R_{ct}) are presented in Fig. 10. It shows that the TEM model predicts the performance of skutterudite TEM with good accuracy and the mean absolute error for open circuit voltage ($U_{TEM.ocv}$) and power output ($P_{TEM.out}$) are respectively 1% and 5%.

The tuning of TEG model is based on a validated TEM model. The tuning parameters for the TEG model are heat transfer coefficients of hot and cold HXRs (h_{hxr} and h_{cxr}). The TEG model for the integration scenario with 400 TEMs could not be fully validated in the engine test programme; for only 12 TEMs were available for testing and were assembled on a single heat exchange channel. With only a subset of the modules tested, a number of assumptions have to be made in order to predict the full TEG performance. The validation results for the TEG model with 12 TEMs in a WLTP test is presented in Fig. 11. It can be seen that the simulation results for both exhaust-out temperature ($T_{exh.out}$) and power output ($P_{TEG.out}$) correspond well with the measurements. The mean absolute errors are respectively 6.4% and 4.8%. In order to predict the TEG output in the case that 400 TEMs were installed, it is assumed that the h_{hxr} and h_{cxr} are the same as the validated TEG model with 12 TEMs. It is also assumed the both $\dot{m}_{exh}$ and $\dot{m}_{col}$ are evenly distributed in the two channels resulting in the same power output for both two channels.

3.3. TEG integration effects modelling

The paper focuses on the potential impact of the TEG on vehicle performance. Four interaction factors (added weight, added electrical water pump, increased exhaust backpressure and energy loss in DC-DC converter) are considered. In the following subsections these factors are analysed and modelled in turn.

3.3.1. Added weight

The effect of added weight can be easily included in the quasi-static vehicle model by increasing the vehicle mass in the vehicle block.
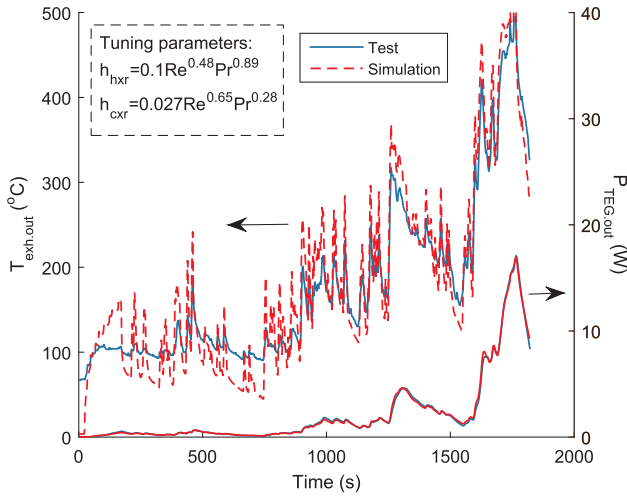
Fig. 11. Validation of the TEG model.

Torque $Tq_{m_{TEG}}$ is added to the original engine torque Tq_{ic} due the increased mass m_{TEG}. Here it is assumed that the total mass of an aluminium TEG system [5] is

$$m_{TEG} = 20 \text{ kg} \tag{14}$$

3.3.2. Added electrical water pump

As can be seen from Fig. 1, an electrical water pump is integrated in the coolant loop of TEG. It circulates the coolant through the cold side of TEG and radiator. Based the data from Ref. [32], 15 W output from an electrical water pump can provide around 0.24 kg/s coolant flow rate. Here it is assumed that power output of the electrical water pump is constant:

$$P_{pump} = 15 \text{ W} \tag{15}$$

3.3.3. Increased exhaust gas backpressure

The backpressure brought by the TEG can lead to an engine power loss. The pressure drop in the hot side HXR can be calculated as [33]:

$$\Delta p = 4f (L/D_f)(\rho_{exh} u_{exh}^2/2) \tag{16}$$

where D_f is the hydraulic diameter; ρ_{exh} and u_{exh} are respectively the density and velocity of the exhaust gas. f is the Darcy resistance coefficient, given in the literature [15]. The power loss of the engine (P_{back}) can be expressed as a function of Δp and ω_{ic} [15].

$$P_{back} = P_{back}(\Delta p, \omega_{ic}) \tag{17}$$

The power losses per pressure drop at different ω_{ic} for a 2L gasoline engine given by Ref. [15] is adapted here.

3.3.4. Energy loss in DC-DC converter

The DC-DC converter is commonly used to convert the voltage supplied by the TEG to reach the voltage levels required by the electrical system in the car. Through a DC-DC converter, a stable voltage can be obtained from the TEG to the in-car electronics. However, the impedance matching between the internal resistance of the TEMs and the input resistance of DC-DC converter can lead to a power loss. Here it is assumed that the efficiency of the DC-DC converter is constant [34]:

$$\eta_{DC-DC} = 90\%. \tag{18}$$

3.4. Fuel saving estimation method

A method to estimate the fuel saving of TEG in light-duty vehicle is proposed in this subsection. The fuel saving is estimated based on $P_{TEG.out}$ and taking the listed four negative integration effects into account.

By taking the effects of added electrical water pump, exhaust back pressure and energy loss in DC-DC converter into account, a modified power output from TEG $P_{TEG.mod}$ can be expressed as:

$$P_{TEG.mod} = P_{TEG.out}\eta_{DC-DC} - P_{back} - P_{pump} \tag{19}$$

Here it is assumed that the power produced by TEG is used to relieve the load on the alternator so as to reduce the original engine torque. Taking the added mass of TEG into consideration ($Tq_{m_{TEG}}$), a modified engine torque profile can be expressed as:

$$Tq_{TEG.ic} = Tq_{ic} + Tq_{m_{TEG}} - \frac{P_{TEG.mod}}{\omega_{ic}\eta_{alt}} \tag{20}$$

η_{alt} is the overall efficiency of the alternator and belt. Here $\eta_{alt} = 50\%$ [35].

By using different engine torque profiles (Tq_{ic} and $Tq_{TEG.ic}$), the cumulated fuel consumptions $E_{fuel}(Tq_{ic})$ and $E_{fuel}(Tq_{TEG.ic})$ can be obtained from the quasi-static vehicle model. Then the fuel saving percentage $\Delta E_{fuel}(\%)$ can be expressed as:

$$\Delta E_{fuel}(\%) = \frac{E_{fuel}(Tq_{ic}) - E_{fuel}(Tq_{TEG.ic})}{E_{fuel}(Tq_{ic})} \times 100\% \tag{21}$$

4. Results and discussion

4.1. Power output potential of TEG in dynamic driving cycles

The results of $P_{TEG.out}$ at different dynamic driving cycles are presented in this subsection. Fig. 12 shows the evolution for the $P_{TEG.out}$ of the two different scenarios at NEDC with average power output. $P_{TEG.out}$ of scenarios 1 is always higher than scenario 2 due to the higher exhaust temperature profile upstream the TWC than the downstream. The exhaust temperature profiles also vary at different driving cycles. In the urban driving cycle average $P_{TEG.out}$ are only 72 W (scenario 1) and 28 W (scenario 2). This can be explained by the low exhaust temperature profile due to the frequent stops at urban driving cycle and relatively lower efficiency of skutterudite modules at low exhaust temperature (300 °C). The average $P_{TEG.out}$ respectively increase to 296 W (scenario 1) and 168 W (scenario 2) in the extra-urban driving cycle when the vehicle runs continuously with high speed. Compared with the NEDC, evolution of the $P_{TEG.out}$ of reference vehicle running FTP-highway cycle is shown in Fig. 13. It can be seen that the TEG shows a quicker response and works more effectively for this high speed driving profile. The average $P_{TEG.out}$ at different driving cycles are presented in Fig. 14. The driving profiles with constant high speed give higher average $P_{TEG.out}$, such as FTP-highway, constant speed 90 km/h and
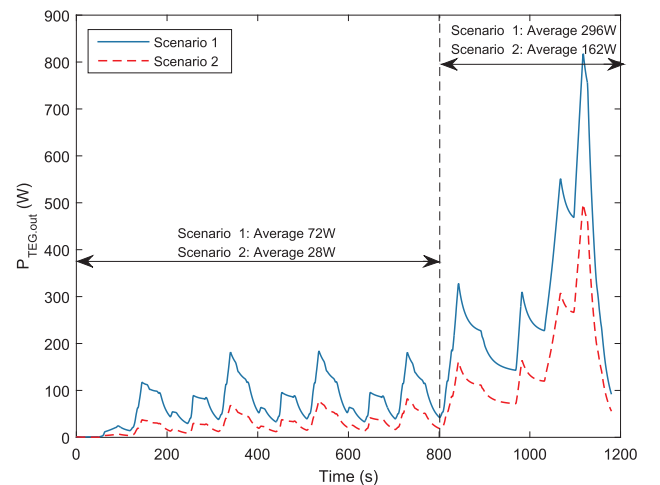

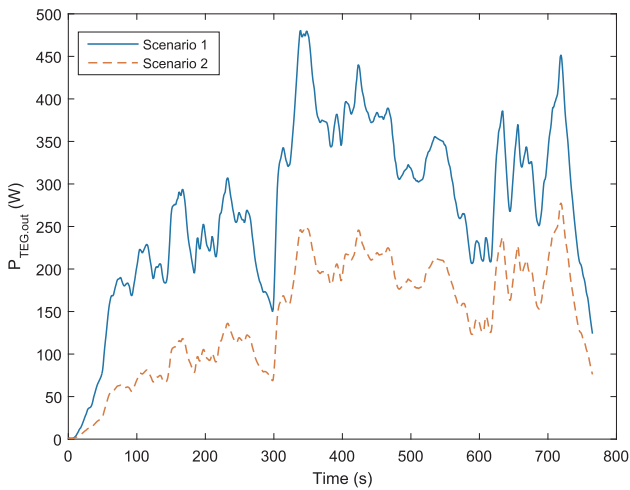**Fig. 12.** Result of $P_{TEG.out}$ at NEDC.

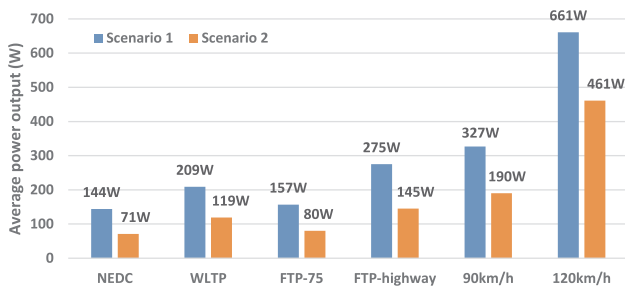Fig. 13. Result of $P_{TEG.out}$ at FTP-highway.

Fig. 14. Average power output at different driving cycles.

120 km/h. The highest average $P_{TEG.out}$ comes from constant speed 120 km/h with average $P_{TEG.out} = 661$ W.

These simulation results of $P_{TEG.out}$ show the skutterudite TEG responds quickly to the exhaust energy change. And it performs effectively with high average $P_{TEG.out}$ when the reference vehicle is running continuously with high speed. However, at the driving cycles with frequent stops and low vehicle speeds the $P_{TEG.out}$ is limited.

4.2. Fuel saving potential of TEG in dynamic driving cycles

By using Eqs. (12)–(14), the fuel saving percentages $\Delta E_{fuel}(\%)$ are estimated based on previous $P_{TEG.out}$. Fig. 15 shows the $\Delta E_{fuel}(\%)$ of scenario 1 and scenario 2 at different driving cycles. The fuel economy improvements between 0.5% and 3.6% depending on integration positions in the exhaust line and driving cycles. $\Delta E_{fuel}(\%)$ of the NEDC and the FTP-75 for both scenarios are relatively lower compared with other driving cycles. The driving cycles of the WLTP, FTP-highway and constant-speed 90 km/h show higher potentials with around 3% of fuel saving for scenario 1 and 1.8% for scenario 2. The constant-speed 120 km/h shows the most promising results for both scenarios: 3.6%
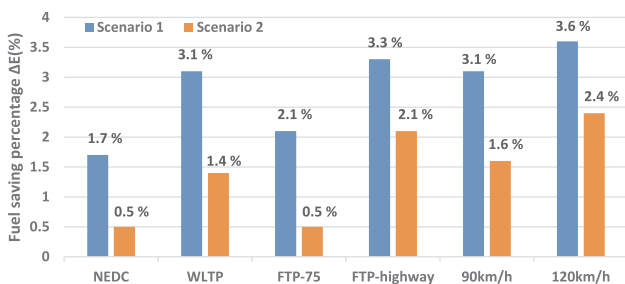

Fig. 15. Fuel saving percentages at different driving cycles.
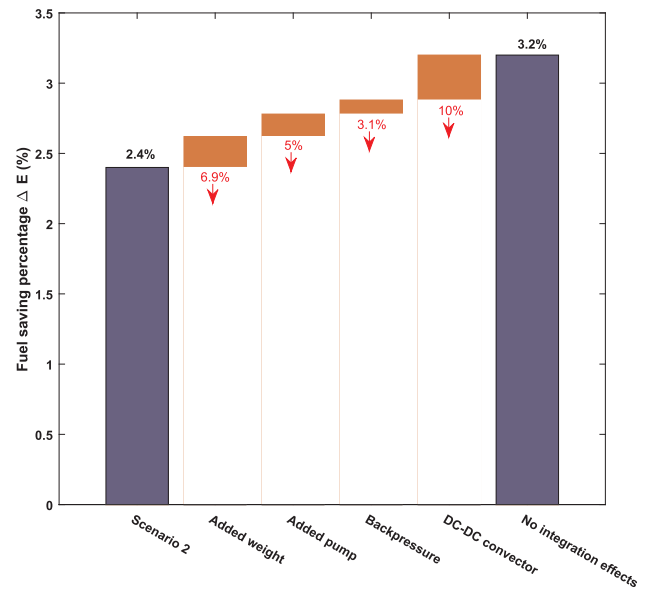

Fig. 16. Influence of the integration effects on fuel saving.

fuel saving for scenario 1 and 2.4% fuel saving for scenario 2. These comparisons further underline that the most promising fuel economy improvement of TEG can obtained when TEG is integrated closer to the engine and running a highway driving cycle.

4.3. Integration effects on fuel saving potential

The integration effects on saving fuel are investigated based on the 120 km/h driving profile for scenario 2. Fig. 16 shows the fuel saving potential of TEG with and without considering the four integration effects. Because of the four integration effects the saving potential is decreased by 25% from $\Delta E_{fuel} = 3.2\%$ to $\Delta E_{fuel} = 2.4\%$. This further underlines the importance and necessity of taking integration effects into consideration when evaluating the fuel saving potential. The contributions of the four integration effects to the decrease of fuel saving percentage are also presented in Fig. 16. The biggest reduction in fuel saving comes from the DC-DC convector, which leads to the 10% decrease in fuel saving. The added weight of TEG is identified as the second biggest reduction of fuel saving (6.9%). In comparison to the previously integration effects, increased exhaust gas backpressure and power consumption in added electrical pump have relatively less significant effects on the fuel saving potential.

4.4. Possibilities of improving fuel saving potential

As shown in Fig. 16, fuel saving potential of the TEG is reduced when considering the TEG installation position and integration effects. The identifications of these effects on fuel saving can be used as a guidance for the optimization of the vehicular TEG. The possibilities of optimizing the vehicular TEG and improving the fuel saving potential are investigated. The different scenarios for TEG integration and their fuel saving percentages are presented in Table 1 and Fig. 17.

From the comparison of scenario 1 and scenario 2, the installation position of the vehicular TEG is identified as one of the main effects on fuel saving potential. Placing the TEG closer to the main exhaust manifold can significantly improve the fuel saving percentage. However, the inlet temperature of the catalytic converter can be influenced by the TEG installed upstream of the TWC resulting in an increased pollutant release [20]. Furthermore, the temperature limits of the TEMs also need to be considered. To solve these issues, a module-based temperature control of bypass valve has been proposed by Loughborough University [22], which can be used to ensure the safely

Table 1
Different integration scenarios of TEG.

	Scenario 2	Scenario 1	Scenario 1(A)	Scenario 1(B)
TEG position	Downstream TWC	Upstream TWC	Upstream TWC	Upstream TWC
Added weight	20 kg	20 kg	15 kg	15 kg
Efficiency of DC-DC convector	90%	90%	95%	95%
Added electrical pump	15 W	15 W	15 W	12 W
Increased backpressure	800–1000 Pa	800–1000 Pa	800–1000 Pa	640–800 Pa
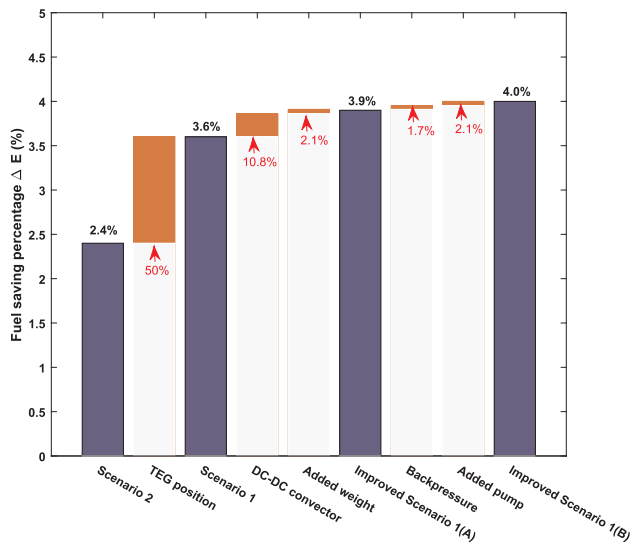
Fig. 17. Effects of different improvement on fuel saving potential in the 120 km/h driving profile.

operation of TEG and effectively operation of catalytic converter. Taking the 120 km/h driving profile as an example, placing the TEG downstream of the CCC can increase the fuel saving by 50% from $\Delta E_{fuel} = 2.4\%$ (downstream of the TWC) to $\Delta E_{fuel} = 3.6\%$.

The efficiency of DC-DC convector and added weight are the main contributors for the reduction of fuel saving potential among the four integration effects. A two-stage cascade boost converter topology was proposed by Ni [36] and the average efficiency of DC-DC convector could be around 95%. A weight reduction can be possibly achieved by optimizing the wall thickness of HXRs [37]. A reduced TEG weight of 15 kg and $\eta_{DC-DC} = 95\%$ are assumed here. Fig. 17 shows the improvements of these two integration effects together can increase ΔE_{fuel} from 3.6% (Scenario 1) to 3.9% (improved Scenario 1(A))

The power consumption in added electrical pump and exhaust backpressure are respectively related to the performance of the cold side HXR and the hot side HXR. Increasing the pumping power consumption, which is proportional to the coolant flow rate, can increase the temperature difference of the modules and the power output of the TEG. Likewise, increasing the heat transfer coefficient of hot side HXR can also lead to an increase of exhaust backpressure. Furthermore, different engine's speeds and torques require different optimal coolant flow rates [35]. Thus, to reduce the effects of added pump and exhaust backpressure on fuel saving, a system level comprehensive optimization of HXRs [38] and a coolant pump control strategy is suggested. It assumed through these methods the exhaust backpressure can decrease 20% and electric pump power is reduced to 12 W while maintaining the heat transfer coefficients of hot and cold side HXRs unchanged. Fig. 17 shows the improvements of these two integration effects can increase ΔE_{fuel} from 3.9% (improved Scenario 1(A)) to 4.0% (improved Scenario

1(B)).

In total, the fuel saving potential increases by 66.7% from $\Delta E_{fuel} = 2.4\%$ (Scenario 2) to $\Delta E_{fuel} = 4.0\%$ (Improved Scenario 1(B)). 50% of this improvement is contributed to installing TEG closer to the exhaust manifold. The second biggest increase in fuel saving potential comes from higher efficiency of DC-DC convector. Reducing the added weight of TEG and decreasing power consumption of electrical pump and backpressure only have a minor increase on fuel saving potential.

5. Conclusions

A method for predicting the fuel saving potential of a skutterudite TEG in light-duty vehicle application was developed and presented in this paper. By building and validating a quasi-static vehicle model, a dynamic exhaust model, a dynamic coolant model and a dynamic TEG model, a semi-empirical model was developed. Based on the semi-empirical model, the fuel saving percentage of TEG was then estimated by taking the integration effects of added weight, added electrical pump, exhaust backpressure and energy loss in DC-DC converter into account. Then these four integration effects on the fuel saving were studied individually and possibilities to increase the fuel saving potential were also investigated.

By comparing the power outputs and fuel saving of TEG in different driving cycles, it was found out the skutterudite TEG has better performance in highway driving than city driving cycle. From the comparison of two TEG integration scenarios, the TEG installation position was identified as the most important effect to the fuel saving potential. The skutterudite equipped TEG permits a higher operating temperature and the possibility of positioning it closer to the engine increases the fuel saving potential by 50%. The listed four integration effects altogether lead to a 25% reduction of fuel saving potential. Among the four integration effects, the energy loss in the DC-DC converter and the added mass due to the TEG were most significant at 10% and 6.9% respectively. The losses due to electrical pump load and the effect of exhaust back pressure had a minor effect at 5% and 3.1% respectively. Based on these identifications, possible methods of optimizing TEG integration scenario, such as bypass valve control strategy, optimization of the HXRs, mass reduction, coolant pump control strategy, can be deployed. Relative to scenario 2, the fuel saving potential was improved by 67% and 4% fuel consumption reduction was achieved at a steady vehicle speed of 120 km/h.

Appendix A. Specification of reference car and TEG

See Tables A.2–A.4.

Table A.2
Specification for reference car.

Total mass of the vehicle [kg]	1520
Frontal area [m]	2.26
Tyre radius [m]	0.326
Drag coefficient [–]	0.29
Transmission ratio 1st to 5th gear [–]	3.66/2.05/1.42/1.06/0.85
Differential gear [–]	3.75
Engine type	Gasoline
Displacement [L]	1.984
Engine maximum power [kW]	150
Engine maximum torque [Nm]	282

Table A.3
Specification for TEG.

TEG weight [kg]	20 kg
Number of hot side HXRs [–]	2
Dimension of hot side HXR [cm]	$24 \times 17 \times 1.6$
Number of cold side HXRs [–]	3
Dimension of cold side HXR [cm]	$24 \times 17 \times 1.6$
Number of fins in a HXR [–]	75
Fin thickness [cm]	0.032
Totally number of TEMs [–]	400
Dimension of a TEM [cm]	$1.6 \times 1.3 \times 0.4$
Hydraulic diameter of hot side HXR [cm]	0.13

Table A.4
Specification for skutterudite module.

Area of a ceramic plate ($10^{-6} \cdot m^2$)	16×13
Area of a thermocouple ($10^{-6} \cdot m^2$)	1.7×1.7
Thickness of a thermocouple ($10^{-3} \cdot m$)	2.2
Thickness of a ceramic plate ($10^{-3} \cdot m$)	0.93
Thickness of a TEM ($10^{-3} \cdot m$)	4.2
Number of thermocouples	9
Thermal conductivity of the ceramic plate ($10^{-5} \cdot W/(m\,K)$)	$k_p = -3.77T^2 + 1.60T + 1.38$ $k_n = 9.94T^2 - 1.11T + 6.22$
Seebeck coefficient of the thermal elements ($10^3 \cdot V/K$)	$S_p = -2.17T^2 + 3.66T + 1.94$ $S_n = 9.94T^2 - 1.11T + 6.22$
Electric conductivity of the thermal elements (S/m)	$\sigma_p = 0.1025T^2 - 181.5T + 192825$ $\sigma_n = 0.0981T^2 - 162.74T + 160395$

References

[1] Yang Z, PradoGonjal J, Phillips M, Lan S, Powell A, Vaqueiro P, et al. Improved thermoelectric generator performance using high temperature thermoelectric materials. Tech. rep. SAE Technical Paper; 2017.

[2] Peng Z, Wang T, He Y, Yang X, Lu L. Analysis of environmental and economic benefits of integrated exhaust energy recovery (eer) for vehicles. Appl Energy 2013;105:238–43.

[3] Agudelo AF, García-Contreras R, Agudelo JR, Armas O. Potential for exhaust gas energy recovery in a diesel passenger car under european driving cycle. Appl Energy 2016;174:201–12.

[4] Fu J, Liu J, Feng R, Yang Y, Wang L, Wang Y. Energy and exergy analysis on gasoline engine based on mapping characteristics experiment. Appl Energy 2013;102:622–30.

[5] Stobart RK, Wijewardane A, Allen C. The potential for thermo-electric devices in passenger vehicle applications. Tech. rep. SAE Technical Paper; 2010.

[6] Twigg MV. Progress and future challenges in controlling automotive exhaust gas emissions. Appl Catal B: Environ 2007;70(1-4):2–15.

[7] Bass JC, Elsner NB, Leavitt FA. Performance of the 1 kw thermoelectric generator for diesel engines. In: AIP conference proceedings, vol. 316, AIP; 1994. p. 295–8.

[8] Ikoma K, Munekiyo M, Furuya K, Kobayashi M, Izumi T, Shinohara K. Thermoelectric generator for gasoline engine vehicles using bi2te3 modules. J Jpn Inst Metals 1999;63(11):1475–8 Special Issue on Thermoelectric Energy Conversion Materials.

[9] Thacher E, Helenbrook B, Karri M, Richter CJ. Testing of an automobile exhaust thermoelectric generator in a light truck. Proc Inst Mech Eng, Part D: J Automob Eng 2007;221(1):95–107.

[10] García-Cañadas J, Powell AV, Kaltzoglou A, Vaqueiro P, Min G. Fabrication and evaluation of a skutterudite-based thermoelectric module for high-temperature applications. J Electron Mater 2013:1–6.

[11] Nie G, Suzuki S, Tomida T, Sumiyoshi A, Ochi T, Mukaiyama K, et al. Performance of skutterudite-based modules. J Electron Mater 2017;46(5):2640–4.

[12] Rowe D, Smith J, Thomas G, Min G. Weight penalty incurred in thermoelectric recovery of automobile exhaust heat. J Electron Mater 2011;40(5):784–8.

[13] Bo Lia YYYLSTJZ, Huang Kuo. Heat transfer enhancement of a modularised thermoelectric power generator for passenger vehicles. Appl Energy 2017;205:868–79.

[14] Deng Y, Liu X, Chen S, Xing H, Su C. Research on the compatibility of the cooling

unit in an automotive exhaust-based thermoelectric generator and engine cooling system. J Electron Mater 2014;43(6):1815.

[15] He W, Wang S. Thermoelectric performance optimization when considering engine power loss caused by back pressure applied to engine exhaust waste heat recovery. Energy 2017;133:584–92.

[16] Cao D, Peng FZ. Multiphase multilevel modular dc–dc converter for high-current high-gain teg application. IEEE Trans Ind Appl 2011;47(3):1400–8.

[17] Yu S, Du Q, Diao H, Shu G, Jiao K. Start-up modes of thermoelectric generator based on vehicle exhaust waste heat recovery. Appl Energy 2015;138:276–90.

[18] Liang X, Sun X, Tian H, Shu G, Wang Y, Wang X. Comparison and parameter optimization of a two-stage thermoelectric generator using high temperature exhaust of internal combustion engine. Appl Energy 2014;130:190–9.

[19] He W, Wang S, Yue L. High net power output analysis with changes in exhaust temperature in a thermoelectric generator system. Appl Energy 2017;196:259–67.

[20] Vázquez J, Sanz-Bobi MA, Palacios R, Arenas A. State of the art of thermoelectric generators based on heat recovered from the exhaust gases of automobiles. In: Proc. 7th European workshop on thermoelectrics, no. 17; 2002.

[21] LeBlanc S, Yee SK, Scullin ML, Dames C, Goodson KE. Material and manufacturing cost considerations for thermoelectrics. Renew Sustain Energy Rev 2014;32:313–27.

[22] Lan S, Yang Z, Chen R, Stobart R. A dynamic model for thermoelectric generator applied to vehicle waste heat recovery. Appl Energy 2018;210:327–38.

[23] Guzzella L, Amstutz A. The qss toolbox manual, ETH Zürich. <http://www.imrt.ethz.ch/research/qss>.

[24] Eriksson L. Mean value models for exhaust system temperatures. Tech. rep., SAE Technical Paper; 2002.

[25] Yoo IK, Simpson K, Bell M, Majkowski S. An engine coolant temperature model and application for cooling system diagnosis. Tech. rep., SAE Technical Paper; 2000.

[26] Lan S, Rouaud C, Stobart R, Chen R, Yang Z, Zhao D. The potential of thermoelectric generator in parallel hybrid vehicle applications. Tech. rep., SAE Technical Paper; 2017.

[27] Sciarretta A, Back M, Guzzella L. Optimal control of parallel hybrid electric

[28] Morra E, Spessa E, Ciaravino C, Vassallo A. Analysis of various operating strategies for a parallel-hybrid diesel powertrain with a belt alternator starter. SAE Int J Alternat Powertrains 2012;1:231–9. [2012-01-1008].

[29] Audi a4. https://www.audiworld.com/model/a4/07/A4_tech.pdf [accessed: 2017-11-10].

[30] Lan S, Yang Z, Stobart R, Winward E. The influence of thermoelectric materials and operation conditions on the performance of thermoelectric generators for automotive. Tech. rep., SAE Technical Paper; 2016.

[31] Farrant P, Robertson A, Hartland J, Joyce S. The application of thermal modelling to an engine and transmission to improve fuel consumption following a cold start. Tech. rep., SAE Technical Paper; 2005.

[32] Tasuni MLM, Latiff ZA, Nasution H, Perang MRM, Jamil HM, Misseri MN. Performance of a water pump in an automotive engine cooling system. Jurnal Teknologi 2016;78(10–2):47–53.

[33] Mavridou S, Mavropoulos G, Bouris D, Hountalas D, Bergeles G. Comparative design study of a diesel exhaust gas heat exchanger for truck applications with conventional and state of the art heat transfer enhancements. Appl Therm Eng 2010;30(8):935–47.

[34] Li M, Xu S, Chen Q, Zheng L-R. Thermoelectric-generator-based dc–dc conversion networks for automotive applications. J Electron Mater 2011;40(5):1136–43.

[35] Karri M, Thacher E, Helenbrook B. Exhaust energy conversion by thermoelectric generator: two case studies. Energy Convers Manage 2011;52(3):1596–611.

[36] Ni L-x, Sun K, Wu H-f, Chen Z, Xing Y. A high efficiency step-up dc-dc converter for thermoelectric generator with wide input voltage range. 2012 IEEE International Symposium on Industrial Electronics (ISIE). Springer; 2012. p. 52–7.

[37] Singh S, Sørensen K, Simonsen AS, Condra TJ. Implications of fin profiles on overall performance and weight reduction of a fin and tube heat exchanger. Appl Therm Eng 2017;115:962–76.

[38] Liu C, Deng Y, Wang X, Liu X, Wang Y, Su C. Multi-objective optimization of heat exchanger in an automotive exhaust thermoelectric generator. Appl Therm Eng 2016;108:916–26.